iScience

CellPress
OPEN ACCESS

Article

Optical multiband polarimetric modulation sensing for gender and species identification of flying native solitary pollinators

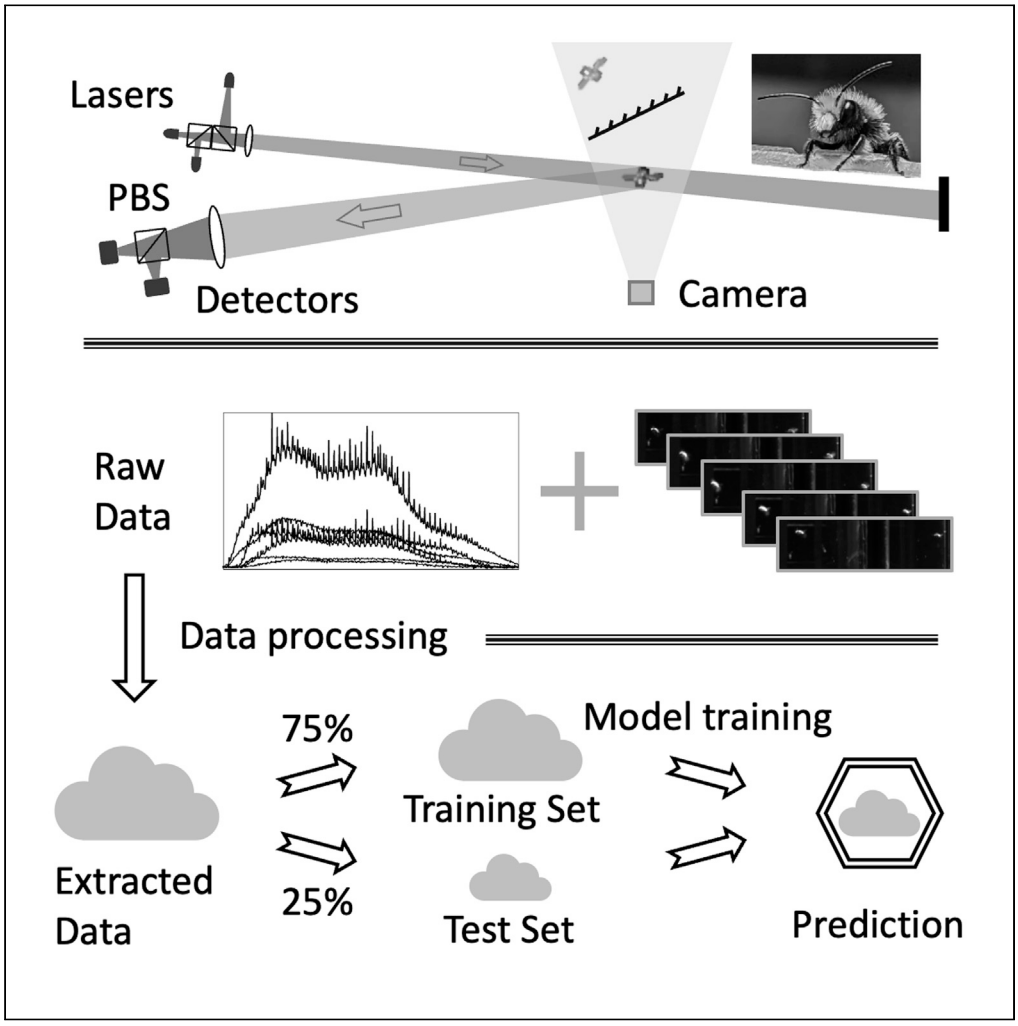

Yiyun Li, Zehua Han, Reed Nessler, ..., Robert Brick, Alexei V. Sokolov, Marlan O. Scully

yiyunli@tamu.edu

Highlights

First attempt to identify flying native solitary pollinators with optical methods

Common species of native solitary pollinators under the same genus are studied

Seasonal activity and foraging preference information improve classification accuracy

Highest classification accuracies on species with overlap exceed 96% and 93%

Li et al., iScience 26, 108265
November 17, 2023 © 2023
https://doi.org/10.1016/j.isci.2023.108265

iScience

CellPress
OPEN ACCESS

Article

Optical multiband polarimetric modulation sensing for gender and species identification of flying native solitary pollinators

Yiyun Li,[1,4,*] Zehua Han,[1] Reed Nessler,[1] Zhenhuan Yi,[1] Philip Hemmer,[1,2] Robert Brick,[1] Alexei V. Sokolov,[1,3] and Marlan O. Scully[1,3]

SUMMARY

Native pollinators are crucial to local ecosystems but are under threat with the introduction of managed pollinators, e.g., honeybees (*Apis mellifera*). We explored the feasibility of employing the entomological lidar technique in native pollinator abundance studies. This study included individuals of both genders of three common solitary bee species, *Osmia californica*, *Osmia lignaria*, and *Osmia ribifloris*, native to North America. Properties including optical cross-section, degree of linear polarization, and wingbeat power spectra at all three wavelengths have been extracted from the insect signals collected by a compact stand-off sensing system. These properties are then used in the classification analysis. For species with temporal and spatial overlapping, the highest accuracies of our method exceed 96% (*O. ribifloris* & *O. lignaria*) and 93% (*O. lignaria* & *O. californica*). The benefit of employing the seasonal activity and foraging preference information in enhancing identification accuracy has been emphasized.

INTRODUCTION

The employment of managed pollinators in agricultural applications can be traced back to ancient times. Honeybees, the most famous managed pollinators, were introduced to North America nearly 400 years ago.[1] Although they are still the most widely used managed pollinators in North America, recent studies have shown that pollinator diversity is beneficial in crop yield outcomes.[2–5] For certain pollinator–dependent crops, it is visitation and pollination of wild bees, not honeybees, that increases crop yield.[6,7] Possible negative consequences of the massively introduced managed pollinators, e.g., honeybees, include competition with native pollinators for floral resources, competition for nest sites, and co-introduction of natural enemies, particularly pathogens.[1] The large foraging distance of honeybees intensifies its competition with native pollinators over floral resources.[8] Moreover, the preference that some nonnative bees have to pollinate nonnative forbs helps invasive weedy species outcompete native wildflowers for pollination services.[3]

The identification and monitoring of potentially, several interacting species of pollinators is urgently needed as a first task for a clear understanding of this important process. The three most–used passive sampling techniques are bowl traps (or pan traps), netting, and nonlethal observation. Despite the increasing number of research works employing bowl trapping in recent years, it has intrinsic drawbacks, e.g., taxonomic bias and an inability to provide reliable estimates of population abundance.[9] Netting and nonlethal observation are labor intensive and entail a strong interference with the insects.

Efforts have been made toward automatic insect monitoring. Automated Insect identification based on its properties is the first step. Wingbeat frequency, the most apparent and readily available property of any flying insects, has been used to distinguish among different species of insects. Based on the methods of picking up the signal, wingbeat frequency measurement techniques can be divided into optoelectronic and acoustic approaches.[10–12] It has been proposed that the difference in the wingbeat frequency obtained from acoustic signals of bees in flight can be used to distinguish Africanized honeybees from European honeybees,[10] however, the detection range of this method is rather limited. And it has been shown that the performance of optoelectronic methods is comparable to the acoustic–sensing approach while less vulnerable to ambient noise.[11] When multiple similar species of insects are included in a study, the precision of wingbeat frequency–based species identification decreases.[12] The wingbeat frequency of insects from different species could be very close, as shown in the table of wingbeat frequency of different homopterous species.[13] Insect identification based on image processing can be considered a digital version of the traditional morphological taxonomy. With the development of Internet of Things (IoT) techniques, image processing applied to trapped insects can improve the temporal resolution of trapping and avoid time–consuming, manual classification of trapped insects.[14] Artificial intelligence aided image processing has been proven to be powerful in distinguishing bees and bee mimics.[15] Techniques such

[1]Institute for Quantum Science and Engineering, Department of Physics and Astronomy, Texas, A&M University, College Station, TX 77843–4242, USA
[2]Department of Electrical & Computer Engineering, Texas, A&M University, College Station, TX 77843–3127, USA
[3]Department of Physics, Baylor University, Waco, TX 76798, USA
[4]Lead contact
*Correspondence: yiyunli@tamu.edu
https://doi.org/10.1016/j.isci.2023.108265

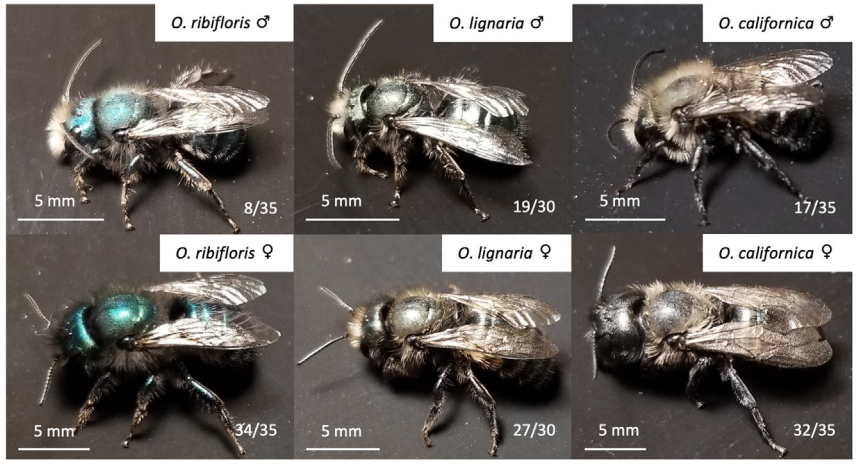

Figure 1. Images of the solitary pollinators used in the study: *O. ribifloris*, *O. lignaria*, and *O. californica*

as computer vision and deep learning have also been employed in real-time insect tracking and monitoring.[16] Spectral information has also been employed in hyperspectral image analysis for fruit fly infestation detection in mango.[17] However, limitations such as bias in trapping constrain its application in biodiversity studies. In scenarios such as pest control where only the families or orders of pests are of interest, silhouettes of the flying pests could be enough for the purpose.[18,19] Then, techniques such as in–line holography can be employed and a large probing volume with a reasonably good probing distance could be expected.[20] Vertical–looking insect radars are an important tool to monitor insects in migration. It has been shown that special–purpose insect radar has the potential to distinguish 23 species of migratory insects with an identification accuracy higher than 80%.[21] But these techniques are less helpful in monitoring similar non–migratory insect species. Recently–developed optical sensing methods have proven to be powerful in distinguishing similar moths and mosquito species, and even gravid and nongravid individuals.[22–24] With the newly–proposed fluorescence hyperspectral lidar, the conventional, time–consuming, mark–recapture process can now be conducted in a very efficient manner, which greatly facilitates the monitoring of the behavior of social insects.[25]

Solitary pollinators, unlike their social relatives, do not live in large colonies but instead raise their offspring on their own. Nests are constructed in existing holes. With the spread–out nests of solitary bees, the mark–recapture process would be very time–consuming. To measure the abundance of solitary pollinators, a system should be capable of distinguishing similar species in the field. In this article, we will explore how optical and polarimetric properties together with the wingbeat frequency can help in the identification of three commercially available native *Osmia* bee species of both genders.

RESULTS AND DISCUSSION

Raw data presentation and interpretation

The classification of each species shown in Figure 1 starts by analyzing the raw data of each insect's transient events recorded in the six channels from the setup shown in Figure 2. Information, i.e., wingbeat power spectra, the optical cross-section of the insect body, and degree of linear polarization (DoLP), were extracted from these raw data and used for classification. With least absorption from melanin and highest responsivity of the InGaAs detectors, signals at 1320 nm have the highest SNR. The time window for each insect transient event at all three wavelengths was determined based on the signal at 1320 nm. The threshold for selecting the insect signals from the raw data was set based on the static median (I_{median}) and the interquartile range (I_{IQR}), ~2.3 times the symmetric Gaussian readout noise amplitude:[26]

$$I_{th} = I_{median} + 8 \times I_{IQR} \quad \text{(Equation 1)}$$

Any part of the raw data whose intensity exceeds the threshold was selected for further study.

Multiband polarimetric signals recorded when an *O. californica* passed through the FOV are shown in Figure 3. The signal intensity was calibrated by randomly dropping a quarter inch (6.35 mm) diameter Teflon ball into the FOV and calculating the average intensity of the recorded Teflon ball signals. The starting and ending moments of signals at different wavelengths are different, showing a mismatch of the boundaries of different laser beams. This indicates that special attention should be paid if the spectral ratio is to be obtained from the signals. Optical cross-section of the *O. californica* in this transit is highest at 1320 nm and lowest at 915 nm, presenting a strong wavelength dependence, as shown in Figure 3A. Wing beats are clear in the signals at all three wavelengths in the co–polarization channel while unexpected dips can be seen in both co– and de–polarization channels. Body contribution for each signal was calculated by using asymmetric least squares (AsLS), shown in Figure 3B, which is commonly used in Raman spectroscopy.[27] This method avoids the artificial kinks seen in previous studies when the body contribution was estimated from the local minima of the signal.[24,28] Efforts have been made to explore power spectral properties, see Figure 3C Zero–filling has been used to increase the apparent frequency resolution to 1 Hz in the fast Fourier transform (FFT) while a

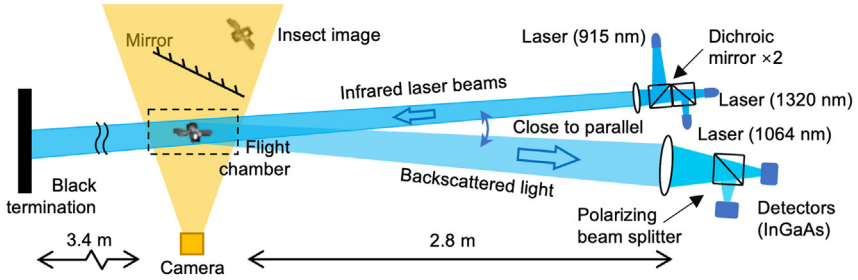

Figure 2. Schematic diagram of the indoor stand-off sensing setup for collecting lidar–like signals containing optical multi–band polarimetric properties of flying solitary pollinators (not to scale)

Hamming window of 120 sample points (40 ms) with 50% overlap was used for Welch's power spectral density (PSD).[29] The fundamental wingbeat frequency of the *O. californica* male signal is 184 Hz, as can be seen from the FFT result. Two large sidebands can be observed in the FFT result while there is only one large and broad band in the result of Welch's method, covering the range of several strong peaks around the fundamental frequency in the FFT curve. While Welch's method (with a narrow window and low-frequency resolution) is widely used in the recent insect wingbeat signal analysis, it is worth knowing that the relatively long signals may contain information regarding the flying status of the insects. It is advisable to explore more of it. We believe a better understanding of the insect signal can help establish the connection between the observation aspects and the properties of the wingbeat signal.

Specular reflection accounts for the strong peaks in the insect signal and such sharp peaks are rarely observed in the de–polarization channel. This is also the reason that wingbeat modulation is weak in the de–polarization signals. However, the sharp dips in Figure 3B indicate an interesting mechanism behind this unusual phenomenon. The wingbeat signals in both co– and de–polarization channels are shown in Figure 4D. Dips in both polarization channels overlap with high consistency. A reasonable hypothesis is that part of the laser irradiating the insect was

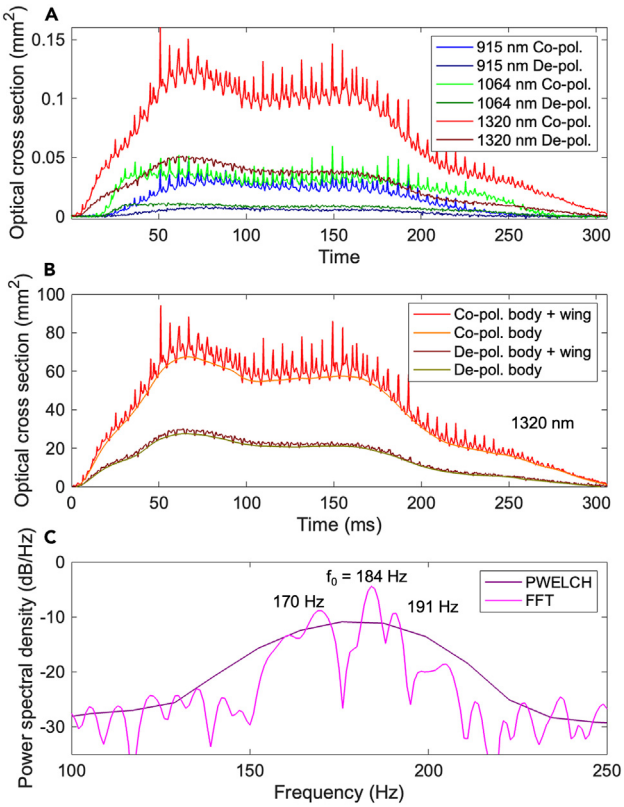

Figure 3. Multiband polarimetric signals of an *O. californica* male passing through the FOV

The signal at three wavelengths in the co–polarization channel and the de–polarization channel is shown in (A), and the signals at 1320 nm in both polarization channels with body fitting are shown in (B). The power spectral density (PSD) of the signal at 1320 nm in co–polarization channel is demonstrated in (C).

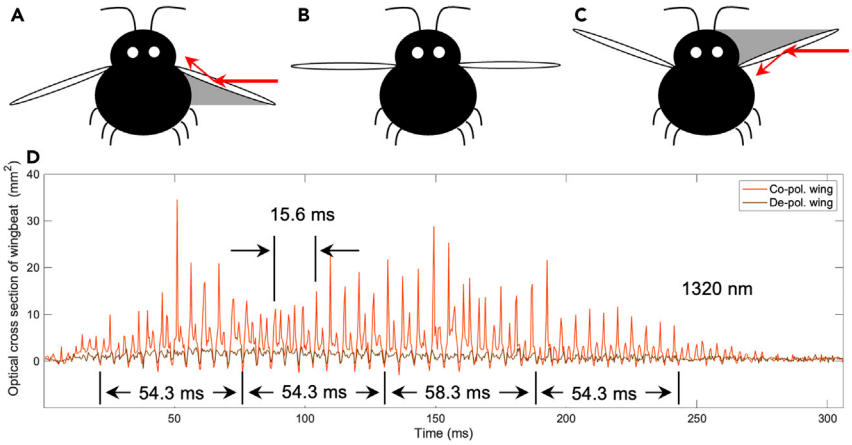

Figure 4. Detailed analysis of wingbeat signals from the *O. californica* male

Hypothesis for the dips in both co–polarization and de–polarization channels (A) bottom of the insect body will be partially blocked by the wing, (B) no blocking from the wing as it is parallel to the laser beam, and (C) top of the insect body will be partially blocked by the wing. The optical cross–section of wingbeat modulation in both co–polarization and de–polarization channels are shown in (D), where we can see a clear overlap of the dips in both polarization channels. The duration of different numbers of wingbeat periods (ten for the bottom numbers and three for the top) has also been given in (D).

reflected away by the specular reflection on the wings, and thus the transparent wing can lead to a sharp dip in the insect signal. When the wing of the insect is in the position shown in Figure 4A, part of the insect body is blocked by the wing, as illustrated by the shadow. Similar blocking can be seen when the wings are in the position in Figure 4C. No blocking will be seen when the wings are parallel to the laser beam, as in Figure 4B. We can see from Figure 1 that the wings of *Osmia* bees grow near the top of their back, which helps explain why there is only one dip in each wingbeat period. The origin of side peaks in Figure 3C can be seen from Figure 4D. Ten periods of wingbeat that last ~54.3 ms suggests a wingbeat frequency of ~184 Hz, the fundamental frequency. Ten periods of wingbeat that last 58.3 ms indicate a wingbeat frequency of ~170 Hz, the side peak on the left in Figure 3C. Three periods that count ~15.6 ms should result in the side peak of higher frequency at ~191 Hz.

As discussed above, special care is needed when calculating the spectral ratio of the insects. In a previous article, the optical cross-section of the insects was falsefully reported to start from 0 mm^2.[24] This is because the body of the insect was not in the FOV. With the aid of the mirror–camera pair in our stereo setup, we can describe the trajectory of the insect in the FOV, which helps confirm when the insect is in the FOV. The coordinate system was established by placing the *y*–axis along the optical axis of the camera lens, the *x*–axis in the horizontal plane perpendicular to the *y*–axis, and the *z*–axis in the vertical direction. The position of the insect at each moment was described by the 3D coordinates obtained from the center–of–mass points of its images recorded by the camera. The *O. californica* male was observed to change its flight direction while in the FOV, as shown in Figure 5A. This is partly because *Osmia* bees fly fast, and the flight chamber is small. As shown in Figure 5B, the three wingbeat periods, starting from 88.6ms, that contribute to the higher wingbeat components, occurred when the insect decreased its speed and was about to start moving upward; ten wingbeat periods, starting from 130.3ms, that attributed to a lower wingbeat frequency, occurred when the insect kept a relatively constant vertical speed but started to gain horizontal speed. The time-frequency analysis of the wingbeat signal can be further aided by for example the spectrogram approach.[30,31] More efforts should be made to find the connection between the insect posture (or flight status) and these side frequency components that can be detected with our stand-off systems. The boundary of the system FOV is shown as blue dashed lines in Figure 5B. From Figure 5B, we can tell when the *O. californica* male is fully in the FOV.

The minimum value of the body contribution when the insect trajectory is considered in the FOV is set as the threshold for determining which part of the signal will be used for the spectral ratio and optical cross-section discussion. This is because the insect images were affected by the frame of the flight chamber. Partially blocked insect images can lead to wrong coordinates, and thus mislead our conclusion whether the insect was in the FOV. This issue needs to be adjusted for. The region at each wavelength that exceeds the corresponding threshold is marked by the shaded area, and the intersection of these three regions will be used. The spectral ratio will only be meaningful when the insects are in the intersection. Signals at 915 nm are the worst affected by the blocking issue due to the smallest beam size. Signals with the average body cross-section of the intersection region lower than the threshold we set in Equation 1, were screened out and not used for the analysis later. In the case shown in Figure 6, this period starts from ~31ms and ends at ~214ms.

Extracted optical properties of insects in flight

The optical cross-section is the average of the body contribution in the selected period shown in Figure 6. DoLP is defined in the way later in discussion and the median value is used to represent the polarimetric property of the insect.

$$DoLP(t) = \frac{I_{body_{co}}(t)}{I_{body_{co}}(t)+I_{body_{de}}(t)} \quad \text{(Equation 2)}$$

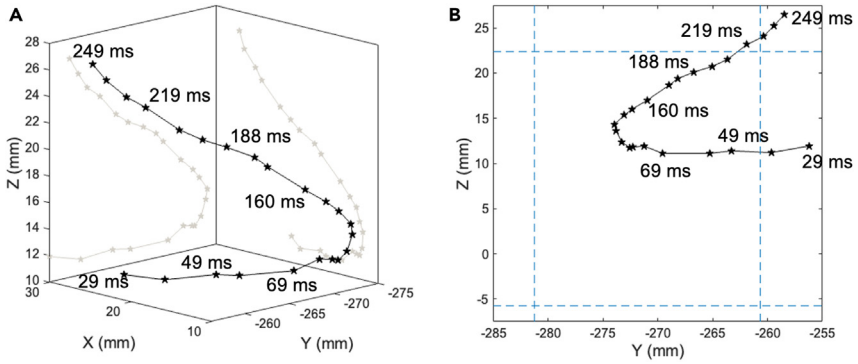

Figure 5. Trajectory and its projection of the *O. californica* male in the FOV

Trajectory of the *O. californica* male in the FOV with its projection in the X–Z and Y–Z planes (A) and its relation to the boundary of the FOV of the system (B).

I_{body_co} and I_{body_de} are the body signal intensity at each moment in the co–polarization channel and de–polarization channel respectively.

It is shown in Figure 7 that the average body optical cross-sections are highest at 1320 nm, and lowest at 915 nm. This is consistent with the result shown in Figure 3. The body cross-section at 1320 nm is comparable to the geometric cross-section of the insects, showing a high

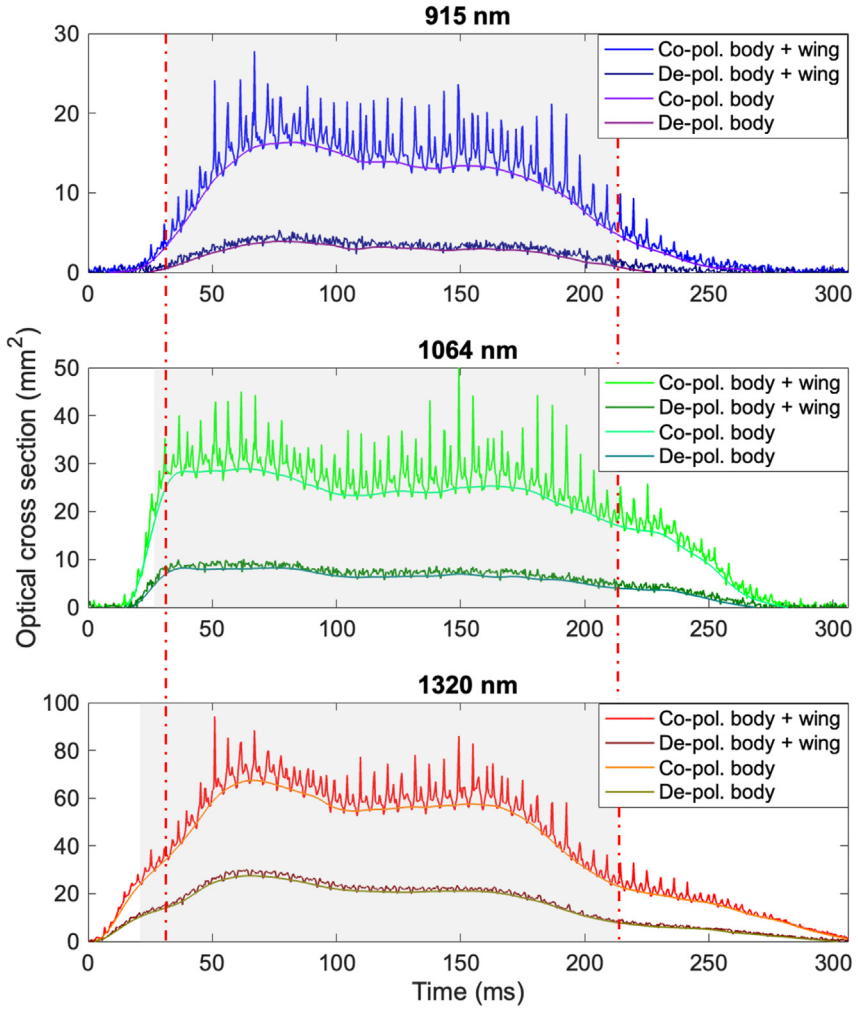

Figure 6. Region of the signal when the *O. californica* male is considered in the FOV at different wavelengths, marked by the shaded area

The overall region that the *O. californica* male is considered in the FOV is marked by the vertical red dash–dotted lines.

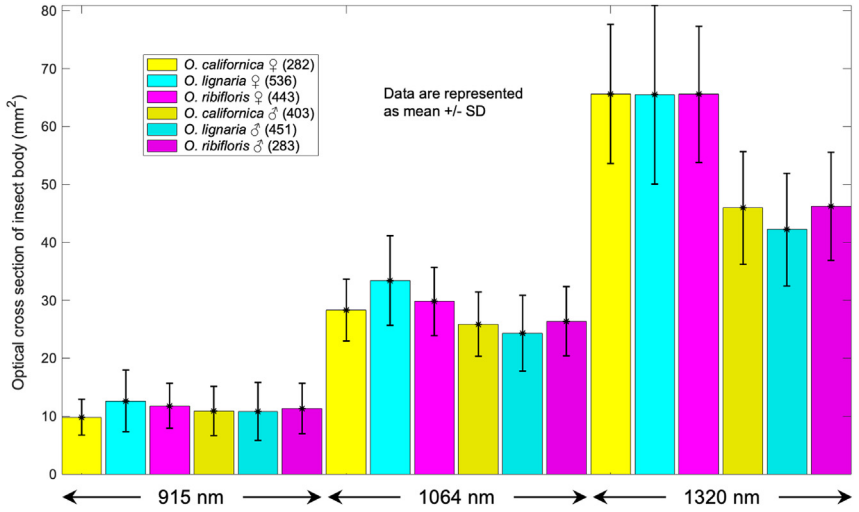

Figure 7. Average of optical cross–section of insect body in flight of six categories at three different wavelengths, with standard deviation on top of the color bar

The number of total signals of each group of insects is shown in the bracket in the legend.

reflectance of these black insects at 1320 nm where melanin has little absorption. Optical cross-sections of females tend to be larger than that of males, which is in good agreement with their actual size. But this difference tends to vanish at 915 nm where strong absorption of melanin can be observed. It also indicates that more light is absorbed by melanin at 915 nm for the females, suggesting a higher amount of melanin in the female individuals. Even though it is hard to observe by the naked eye, our measurement shows that the females are darker than the males, indicating a higher surface concentration of melanin, and thus are less vulnerable to bacteria and fungi, which helps explain the higher survival rate of females in this study.

The DoLP is shown in Figure 8. DoLP is a typical dimensionless quantity that is not significantly affected by laser intensity variation in time and space and is claimed to display little variance among mosquito signals.[24] The highest DoLP is observed at 915 nm, where scattering is expected to be strongest among the three wavelengths used in this study, and the lowest DoLP occurs at 1320 nm, where the scattering coefficient is expected to be the smallest. Considering the absorption of melanin in the multiple scattering process, this phenomenon reveals that absorption dominates the light–melanin interaction in the insects studied in this work. This conclusion agrees with a study on a well–solubilized eumelanin solution.[32]

To explore the origin of the different DoLPs among the same group of insects, two signals at 1320 nm with the lowest and highest DoLP from *O. californica* males are plotted in Figures 9A and 9B with the insect image taken while passing through the FOV in Figures 9C and 9D.

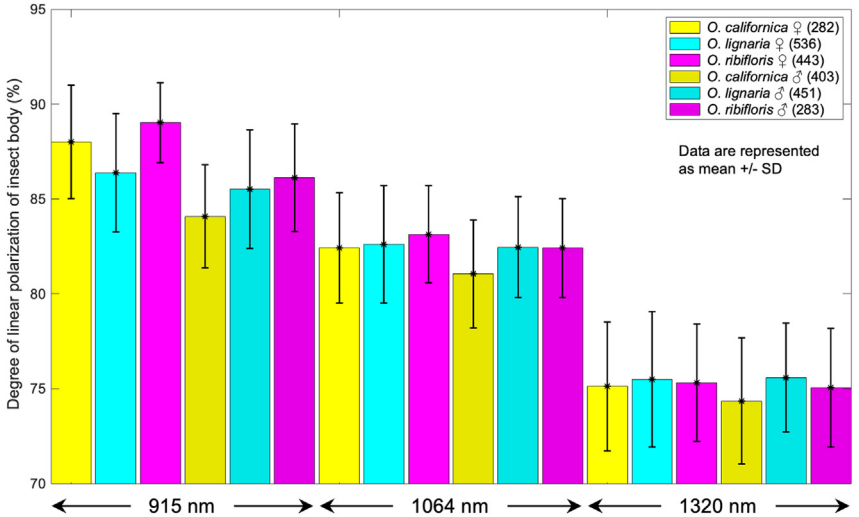

Figure 8. Average DoLP of insect body of six categories in flight at three different wavelengths, with standard deviation on top of the color bar

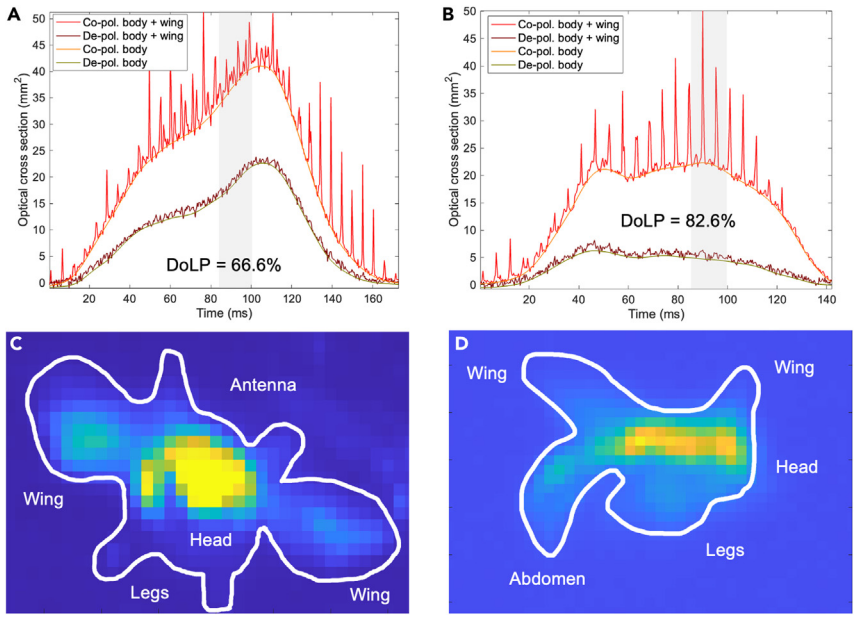

Figure 9. Signals at 1320 nm with the lowest (A) and the highest (B) DoLP of *O. californica* with the images of the insect while passing through the FOV (C) and (D), respectively

The time windows that the insects are considered in the FOV are marked with the shaded regions in (A) and (B). The silhouettes of the insects are marked by the white line in (C) and (D) with different parts of the insects annotated.

The transit that caused the highest DoLP involved an insect that flew toward the lasers and detectors with its furry pubescence facing the laser. And indeed, it has been shown that tiny structures such as hairs display a significantly enhanced co–polarized component, namely, a higher DoLP.[33] In contrast, the transit showing the lowest DoLP happened when the whole hairless abdomen of the *O. californica* male was exposed to the laser beam when the insect's body was perpendicular to the laser. This finding shows that the insect DoLP is still orientation dependent.

Efforts have also been made to extract wingbeat information. As discussed above, due to the limited size of the flight chamber, the insects had to change their flight direction, accelerating, and decelerating often, which leads to sidebands and makes it hard to tell the true fundamental wingbeat frequency in many cases. We used the PSDs from Welch's method for the analysis. Strong deviation can be observed in all six categories of *Osmia* bees, as illustrated in Figure 10. The deviation is relatively small in *O. californica* individuals, which may relate to the impact of the fresh dandelions used in the measurement. A larger flight chamber may help alleviate this strong deviation. The constant change in velocity is analogous to the behavior in the field when the bees are foraging around flowers, which raises the concern that the PSDs can be different between bees heading toward the flowers and flying among them.

Optical cross-sections in the co-polarization channels, DoLP at all three wavelengths, their ratios, and the scores of the first 15 principal components of each wingbeat power spectral density in co-polarization at all wavelengths are used for classification. 75% of the data were used for training the model while the remaining 25% were used as the test set. Results of linear discriminant and four support vector machine (SVM) algorithms installed in the classification learner in MATLAB are shown in Table 1. The highest average accuracy, 86.9%, is achieved with the data of *O. lignaria* females under Median Gaussian SVM. This accuracy may be attributed to its higher optical cross-section and lower DoLP at 915 nm compared to female individuals from the other two species. The lowest classification accuracy is observed in *O. ribifloris* males, partly because of the limited number of individuals surviving for the measurement and of relatively large individual differences. The standard deviation of accuracy is relatively large, which could be attributed to the smaller amount of data collected and the significant individual variance in this study.

However, in the real field applications, we don't necessarily need to distinguish insects among both genders of all three species. As discussed in Sec. 2.1., *O. ribifloris* hatches the earliest in spring while *O. californica* hatches the latest. Plants in the family Ericaceae are generally taller than plants in the family Asteraceae. With the aid of machine learning and multispectral imaging techniques, plant species can be identified in the remote sensing manner.[34] Combining the high spatial resolution of lidar techniques and the typical flight pattern of foraging behavior, pollinators preferring different plants can be distinguished directly by their spatial isolation. It is rational to conclude that *O. ribifloris* and *O. californica* should have little to no overlap in their foraging behavior since they are temporally and spatially isolated. Even though female and male individuals from *O. ribifloris* imbibe nectar, and *O. ribifloris* males can be active throughout the adult activity period, the visitation of male *O. ribifloris* to the flowers is described as "rare" or "substantially less."[35–38] We may ignore them when the probing volume is set close to the flowers of target plants. Although the male individuals of *O. lignaria* tend to hover around the nest waiting for mating, they are also reported to visit blooms.[39,40] Based on the discussion above, it is reasonable to divide the three species into two groups, i.e., *O. ribifloris* & *O. lignaria* and *O. lignaria* & *O. californica* but excluding the *O. ribifloris* males in the classification.

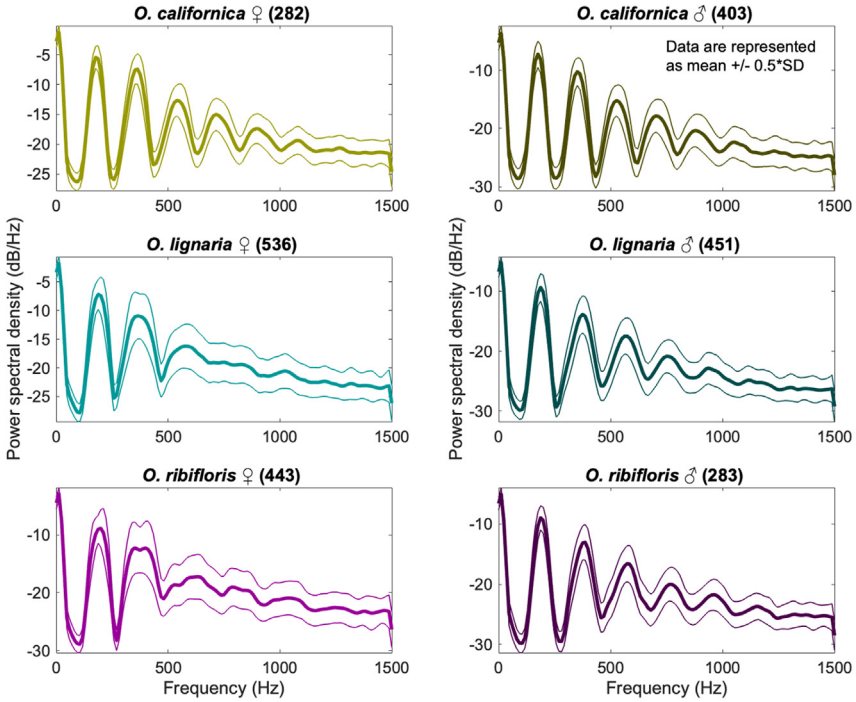

Figure 10. The average PSD of each category of *Osmia* bees at 1320 nm is shown with the central, thick curve, while the standard deviation is marked with two thinner curves of the same color in each subplot

It is shown in Tables 2 and 3 that the classification accuracy of each group of *Osmia* spp. increased has increased compared to the results shown in Table 1. For instance, the classification accuracy of *O. lignaria* males increased more than 10%. It illustrates the importance of considering the natural behavior of the insect of interest in insect classification and biodiversity studies. The classification accuracy of *Osmia lignaria* males in Table 2 is higher than the other two categories of female *Osmia* spp., which indicates that the difference between individuals of different genders of the same *Osmia* species is larger than that between the individuals of the same gender but different species. The classification accuracy of female *Osmia californica* and female *Osmia lignaria* is higher than that of the males in Table 3, which may originate from the relatively less variation in their optical properties such as optical cross-section and degree of linear polarization at different wavelengths. The correlation between the PSD curves and the classification appears dim, which may require more detailed studies.

Conclusion and discussion

This experiment demonstrates the first effort made toward using optical methods to study native pollinator identification and abundance. Relatively good results for a study focused on similar species in one genus have been achieved, with the highest average accuracy of identification exceeding 96% and 93% on pollinators with overlap in time and space. We also reveal the connection between optical properties measured in this stand-off measurement and the insect biological features. It has been shown in this study that not only the spectral ratio and wingbeat pattern but also the DoLP are orientation–dependent, so that it is beneficial to have the heading direction information counted in the classification. The measurement of insects' heading direction in the field has been preliminarily explored in.[41] When the flight velocity in

Table 1. Average classification accuracy of all *Osmia* spp. (with standard deviation in bracket)

	CSVM (%)	LD (%)	LSVM (%)	MGSVM (%)	QSVM (%)
O. californica ♀	78.8 (3.7)	76.4 (4.8)	75.9 (3.5)	70.3 (4.2)	79.6 (3.0)
O. californica ♂	72.1 (3.6)	75.0 (4.2)	75.8 (3.8)	73.8 (3.2)	75.2 (3.2)
O. lignaria ♀	79.9 (2.4)	81.9 (4.2)	83.3 (3.0)	86.9 (2.3)	81.3 (3.0)
O. lignaria ♂	60.9 (5.1)	56.5 (1.8)	68.3 (3.1)	71.0 (2.1)	65.4 (5.1)
O. ribifloris ♀	76.9 (4.4)	75.7 (4.1)	78.0 (4.2)	76.6 (3.5)	79.3 (3.9)
O. ribifloris ♂	47.9 (5.8)	41.8 (3.6)	36.7 (4.9)	39.9 (3.5)	46.0 (5.5)

*CSVM: Cubic SVM; LD: Linear discriminant; LSVM: Linear SVM; MGSVM: Median Gaussian SVM; QSVM: Quadratic SVM.

Table 2. Average accuracy classification of *O. ribifloris* & *O. lignaria* (with standard deviation in bracket)

	CSVM (%)	LD (%)	LSVM (%)	MGSVM (%)	QSVM (%)
O. lignaria ♀	84.8 (2.2)	86.9 (1.5)	85.8 (2.2)	89.0 (1.8)	86.7 (2.4)
O. lignaria ♂	96.5 (1.3)	95.4 (2.4)	96.7 (2.0)	91.7 (2.5)	96.7 (1.5)
O. ribifloris ♀	86.6 (2.4)	84.5 (4.1)	86.1 (2.9)	83.2 (5.1)	86.4 (3.3)

3D is available, the direction of the insects' flight can be interpreted in the field measurement, and thus a higher accuracy in identification can be expected. It is worth pointing out that measuring scattered light from pinned insects is a promising approach to establishing a comprehensive dataset for any insects of interest. However, since the angle between the insects and the horizontal plane is not fixed in flight, we would need to change the way of pinning the insect or scanning at different planes to cover the possible angle range between the insect body and the horizontal plane. Attention should also be paid if "remoisturizing the dry insect" could fully restore the inner structure of insect tissue when measuring the insects with relatively transparent cuticles. If not, fresh samples would be highly preferred in the measurement.

Limitations of the study

Shortcomings of the experiment are also obvious: limited number of insect samples, fixed temperature, imperfect illumination, and a small flight chamber size, which should be improved in future studies. The effects of ambient temperature and relative humidity on *Osmia* bees should also be addressed in future studies. The flight chamber size is constrained in part by the limited depth of field of the surveillance camera, which can be overcome by using the in–line digital holography setup demonstrated in.[20] For further study of *Osmia* bees, our efforts should be made toward utilizing their wingbeat signals since their body can be covered with pollen and the reflectance and polarimetric properties shall be vastly changed. To further study the impact of invasive species, classification work on native *Osmia* bees together with the invasive species that emerge at the same time, use similar floral resources, and have similar nesting habits, e.g., *O. lignaria* with *O. taurus* and *O. cornifrons*, should be further explored.[42]

STAR★METHODS

Detailed methods are provided in the online version of this paper and include the following:

- KEY RESOURCES TABLE
- RESOURCE AVAILABILITY
  - Lead contact
  - Materials availability
  - Data and code availability
- EXPERIMENTAL MODEL AND SUBJECT DETAILS
- METHOD DETAILS
  - Light–insect interaction
  - Experimental setup
- QUANTIFICATION AND STATISTICAL ANALYSIS

ACKNOWLEDGMENTS

The authors are grateful to Mr. Kimball Clark from NativeBees.com who provided the cocoons and offered his expertise in helping us manage the bees in the lab environment. The authors are also grateful to Dr. Theresa L. Pitts–Singer from USDA for her help regarding the suitable humidity level in the experiment. The authors are also grateful to L. L. who helped double–check the format before final submission. Y. L. was first supported by the Herman F. Heep and Minnie Belle Heep Texas A&M University Endowed Fund held/administered by the Texas A&M Foundation and then supported by the Hagler Institute for Advanced Study Heep Graduate Fellowship Award. R. N. and Z. H. were supported by the Herman F. Heep and Minnie Belle Heep Texas A&M University Endowed Fund held/administered by the Texas A&M Foundation. We acknowledge the support of the Air Force Office of Scientific Research (FA9550–20–1–0366); Robert A. Welch Foundation (A–1261, A–1547); Office of Naval Research (N00014–20–1–2184); and King Abdulaziz City for Science and Technology.

Table 3. Average accuracy classification of *O. lignaria* & *O. californica* (with standard deviation in bracket)

	CSVM (%)	LD (%)	LSVM (%)	MGSVM (%)	QSVM (%)
O. californica ♀	90.6 (3.6)	88.7 (4.5)	88.2 (4.8)	80.9 (5.5)	90.5 (3.4)
O. californica ♂	79.4 (4.8)	79.3 (3.7)	79.1 (3.9)	79.2 (5.4)	79.0 (4.2)
O. lignaria ♀	89.8 (3.0)	88.6 (2.7)	90.2 (3.2)	93.4 (1.5)	90.8 (2.4)
O. lignaria ♂	78.2 (2.6)	74.5 (4.8)	77.1 (2.6)	75.2 (3.4)	76.5 (2.7)

AUTHOR CONTRIBUTIONS

Conceptualization, Y.L., A.S., and M.S.; methodology, Y.L. and Z.H.; software, Y.L.; validation, Y.L. and Z.H.; formal analysis, Y.L., R.N., Z.Y., P.H., R.B., and A.S.; investigation, Y.L.; resources, Y.L. and Z.Y.; data curation, Y.L., Z.H., and Z.Y.; writing—original draft preparation, Y.L.; writing—review and editing, R.N., R.B., P.H., and A.S.; visualization, Y.L.; supervision, M.S.; project administration, A.S. and M.S.; funding acquisition, M.S. All authors have read and agreed to the published version of the article.

DECLARATION OF INTERESTS

The authors declare no competing interests.

Received: March 26, 2023
Revised: July 13, 2023
Accepted: October 17, 2023
Published: October 20, 2023

REFERENCES

1. Goulson, D. (2003). Effects of Introduced Bees on Native Ecosystems. Annu. Rev. Ecol. Evol. Syst. *34*, 1–26. https://doi.org/10.1146/annurev.ecolsys.34.011802.132355.
2. Garibaldi, L.A., Carvalheiro, L.G., Vaissière, B.E., Gemmill-Herren, B., Hipólito, J., Freitas, B.M., Ngo, H.T., Azzu, N., Sáez, A., Åström, J., et al. (2016). Mutually beneficial pollinator diversity and crop yield outcomes in small and large farms. Science *351*, 388–391. https://doi.org/10.1126/science.aac7287.
3. Pitts-Singer, T.L., and Cane, J.H. (2011). The Alfalfa Leafcutting Bee, Megachile rotundata: The World's Most Intensively Managed Solitary Bee. Annu. Rev. Entomol. *56*, 221–237. https://doi.org/10.1146/annurev-ento-120709-144836.
4. Vanbergen, A.J., Espíndola, A., and Aizen, M.A. (2018). Risks to pollinators and pollination from invasive alien species. Nat. Ecol. Evol. *2*, 16–25. https://doi.org/10.1038/s41559-017-0412-3.
5. Rader, R., Bartomeus, I., Garibaldi, L.A., Garratt, M.P.D., Howlett, B.G., Winfree, R., Cunningham, S.A., Mayfield, M.M., Arthur, A.D., Andersson, G.K.S., et al. (2016). Non-bee insects are important contributors to global crop pollination. P. Natl. Acad. Sci. USA *113*, 146–151. https://doi.org/10.1073/pnas.1517092112.
6. Mallinger, R.E., and Gratton, C. (2015). Species richness of wild bees, but not the use of managed honeybees, increases fruit set of a pollinator-dependent crop. J. Appl. Ecol. *52*, 323–330.
7. Gibson, S.D., Halvorson, K.S., Myers, L., and Colla, S.R. (2022). Insect visitation and pollination of a culturally significant plant, Hopi tobacco (Nicotiana rustica). iScience *25*, 105613. https://doi.org/10.1016/j.isci.2022.105613.
8. Saunders, M.E., Smith, T.J., Rader, R., and Rader, R. (2018). Bee conservation: Key role of managed bees. Science *360*, 389. https://doi.org/10.1126/science.aat1535.
9. Portman, Z.M., Bruninga-Socolar, B., and Cariveau, D.P. (2020). The State of Bee Monitoring in the United States: A Call to Refocus Away From Bowl Traps and Towards More Effective Methods. Ann. Entomol. Soc. Am. *113*, 337–342. https://doi.org/10.1093/aesa/saaa010.
10. Kerr, H.T., Buchanan, M.E., and Valentine, K.H. (1990). Method and device for identifying different species of honeybees. J. Acoust. Soc. Am. *87*, 2803. https://doi.org/10.1121/1.399014.
11. Potamitis, I., and Rigakis, I. (2015). Novel Noise-Robust Optoacoustic Sensors to Identify Insects Through Wingbeats. IEEE Sens. J. *15*, 4621–4631. https://doi.org/10.1109/JSEN.2015.2424924.
12. Genoud, A.P., Basistyy, R., Williams, G.M., and Thomas, B.P. (2018). Optical remote sensing for monitoring flying mosquitoes, gender identification and discussion on species identification. Appl. Phys. B *124*, 46. https://doi.org/10.1007/s00340-018-6917-x.
13. Byrne, D.N., Buchmann, S.L., and Spangler, H.G. (1988). Relationship Between Wing Loading, Wingbeat Frequency and Body Mass in Homopterous Insects. J. Exp. Biol. *135*, 9–23. https://doi.org/10.1242/jeb.135.1.9.
14. Zualkernan, I.A., Dhou, S., Judas, J., Sajun, A.R., Gomez, B.R., Hussain, L.A., and Sakhnini, D. (2020). Towards an IoT-Based Deep Learning Architecture for Camera Trap Image Classification (IEEE GCAIoT), pp. 1–6. https://doi.org/10.1109/GCAIoT51063.2020.9345858.
15. Bhuiyan, T., Carney, R.M., and Chellappan, S. (2022). Artificial intelligence versus natural selection: Using computer vision techniques to classify bees and bee mimics. iScience *25*, 104924. https://doi.org/10.1016/j.isci.2022.104924.
16. Bjerge, K., Mann, H.M.R., and Høye, T.T. (2022). Real-time insect tracking and monitoring with computer vision and deep learning. Remote Sens. Ecol. Conserv. *8*, 315–327. https://doi.org/10.1002/rse2.245.
17. Haff, R.P., Saranwong, S., Thanapase, W., Janhiran, A., Kasemsumran, S., and Kawano, S. (2013). Automatic image analysis and spot classification for detection of fruit fly infestation in hyperspectral images of mangoes. Postharvest Biol. Tec. *86*, 23–28. https://doi.org/10.1016/j.postharvbio.2013.06.003.
18. Quarles, W. (2018). IPM for Cannabis Pests. IPM Practitioner Monit. Field Pest Manage *36*.
19. Ajayi, O.S., and Samuel-Foo, M. (2021). Hemp Pest Spectrum and Potential Relationship between Helicoverpa zea Infestation and Hemp Production in the United States in the Face of Climate Change. Insects *12*, 940. https://doi.org/10.3390/insects12100940.
20. Hall, M.L., Gleave, K., Hughes, A., McCall, P.J., Towers, C.E., and Towers, D.P. (2022). The application of digital holography for accurate three-dimensional localisation of mosquito-bednet interaction. Light Adv. Manuf. *3*, 1. https://doi.org/10.37188/lam.2022.020.
21. Hu, C., Kong, S., Wang, R., Long, T., and Fu, X. (2018). Identification of Migratory Insects from their Physical Features using a Decision-Tree Support Vector Machine and its Application to Radar Entomology. Sci. Rep. *8*, 5449. https://doi.org/10.1038/s41598-018-23825-1.
22. Li, Y.Y., Zhang, H., Duan, Z., Lian, M., Zhao, G.Y., Sun, X.H., Hu, J.D., Gao, L.N., Feng, H.Q., and Svanberg, S. (2016). Optical characterization of agricultural pest insects: a methodological study in the spectral and time domains. Appl. Phys. B *122*, 213. https://doi.org/10.1007/s00340-016-6485-x.
23. Genoud, A.P., Gao, Y., Williams, G.M., and Thomas, B.P. (2019). Identification of gravid mosquitoes from changes in spectral and polarimetric backscatter cross sections. J. Biophotonics *12*, e201900123. https://doi.org/10.1002/jbio.201900123.
24. Gebru, A., Jansson, S., Ignell, R., Kirkeby, C., Prangsma, J.C., and Brydegaard, M. (2018). Multiband modulation spectroscopy for the determination of sex and species of mosquitoes in flight. J. Biophotonics *11*, e201800014. https://doi.org/10.1002/jbio.201800014.
25. Månefjord, H., Müller, L., Li, M., Salvador, J., Blomqvist, S., Runemark, A., Kirkeby, C., Ignell, R., Bood, J., and Brydegaard, M. (2022). 3D-Printed Fluorescence Hyperspectral Lidar for Monitoring Tagged Insects. IEEE J. Sel. Top. Quant. *28*, 1–9. https://doi.org/10.1109/JSTQE.2022.3162417.
26. Kouakou, B.K., Jansson, S., Brydegaard, M., and Zoueu, J.T. (2020). Entomological Scheimpflug lidar for estimating unique insect classes in-situ field test from Ivory Coast. OSA Continuum *3*, 2362–2371. https://doi.org/10.1364/OSAC.387727.
27. Han, Z., Strycker, B.D., Commer, B., Wang, K., Shaw, B.D., Scully, M.O., and Sokolov, A.V. (2020). Molecular origin of the Raman signal from Aspergillus nidulans conidia and observation of fluorescence vibrational structure at room temperature. Sci. Rep. *10*, 5428. https://doi.org/10.1038/s41598-020-62112-w.
28. Zhu, S., Malmqvist, E., Li, W., Jansson, S., Li, Y., Duan, Z., Svanberg, K., Feng, H., Song, Z., Zhao, G., et al. (2017). Insect abundance over

Chinese rice fields in relation to environmental parameters, studied with a polarization-sensitive CW near-IR lidar system. Appl. Phys. B *123*, 211. https://doi.org/10.1007/s00340-017-6784-x.

29. Welch, P. (1967). The use of fast Fourier transform for the estimation of power spectra: A method based on time averaging over short, modified periodograms. IEEE T. Acoust. Speech *15*, 70–73. https://doi.org/10.1109/TAU.1967.1161901.
30. Cohen, L. (1995). Time-frequency Analysis (Prentice Hall PTR).
31. Deller, J.R., Jr. (1993). Discrete-time Processing of Speech Signals (Macmillan Coll Div).
32. Riesz, J., Gilmore, J., and Meredith, P. (2006). Quantitative scattering of melanin solutions. Biophys. J. *90*, 4137–4144. https://doi.org/10.1529/biophysj.105.075713.
33. Jansson, S., Atkinson, P., Ignell, R., and Brydegaard, M. (2019). First Polarimetric Investigation of Malaria Mosquitoes as Lidar Targets. IEEE J. Sel. Top. Quant. *25*, 1–8. https://doi.org/10.1109/JSTQE.2018.2859225.
34. Paz-Kagan, T., Silver, M., Panov, N., and Karnieli, A. (2019). Multispectral Approach for Identifying Invasive Plant Species Based on Flowering Phenology Characteristics. Remote Sens *11*, 953.
35. Stubbs, C.S., Drummond, F.A., and Osgood, E.A. (1994). Osmia ribifloris biedermannii and Megachile rotundata (Hymenoptera: Megachilidae) Introduced into the Lowbush Blueberry Agroecosystem in Maine. J. Kansas Entomol. Soc. *67*, 173–185. https://www.jstor.org/stable/25085506.
36. Sampson, B.J., and Cane, J.H. (2000). Pollination Efficiencies of Three Bee (Hymenoptera: Apoidea) Species Visiting Rabbiteye Blueberry. J. Econ. Entomol. *93*, 1726–1731. https://doi.org/10.1603/0022-0493-93.6.1726.
37. Torchio, P.F. (1990). Osmia ribifloris, a Native Bee Species Developed as a Commercially Managed Pollinator of Highbush Blueberry (Hymenoptera: Megachilidae). J. Kansas Entomol. Soc. *63*, 427–436. https://www.jstor.org/stable/25085200.
38. Sampson, B.J., Stringer, S.J., Cane, J.H., and Spiers, J.M. (2004). Screenhouse Evaluations of a Mason Bee Osmia ribifloris (Hymenoptera: Megachilidae) as a Pollinator for Blueberries in the Southeastern United States. Small Fruits Rev. *3*, 381–392. https://doi.org/10.1300/J301v03n03_15.
39. Scalici, M.B., McCabe, L.M., Alston, D.G., Peterson, S.S., Yost, M., and Pitts-Singer, T.L. (2023). Blue orchard bee (Hymenoptera: Megachilidae) origin and orchard growing region affect female retention at artificial nest sites in cherry orchards. Environ. Entomol. *52*, 681–691. https://doi.org/10.1093/ee/nvad057.
40. Torchio, P.F. (1976). Use of Osmia lignaria Say (Hymenoptera: Apoidea, Megachilidae) as a Pollinator in an Apple and Prune Orchard. J. Kansas Entomol. Soc. *49*, 475–482. https://www.jstor.org/stable/25082856.
41. Li, Y., Wang, K., Quintero-Torres, R., Brick, R., Sokolov, A.V., and Scully, M.O. (2020). Insect flight velocity measurement with a CW near-IR Scheimpflug lidar system. Opt Express *28*, 21891–21902.
42. LeCroy, K.A., Savoy-Burke, G., Carr, D.E., Delaney, D.A., and Roulston, T.H. (2020). Decline of six native mason bee species following the arrival of an exotic congener. Sci. Rep. *10*, 18745. https://doi.org/10.1038/s41598-020-75566-9.
43. Eilers, P.H., and Boelens, H.F. (2005). Baseline Correction with Asymmetric Least Squares Smoothing, *1* (Leiden University Medical Centre Report), p. 5.
44. Sedivy, C., and Dorn, S. (2014). Towards a sustainable management of bees of the subgenus Osmia (Megachilidae, Osmia) as fruit tree pollinators. Apidologie *45*, 88–105. https://doi.org/10.1007/s13592-013-0231-8.
45. Cripps, C., and Rust, R.W. (1989). Pollen Foraging in a Community of Osmia Bees (Hymenoptera: Megachilidae). Environ. Entomol. *18*, 582–589. https://doi.org/10.1093/ee/18.4.582.
46. Cripps, C., and Rust, R.W. (1989). Pollen Preferences of Seven Osmia Species (Hymenoptera: Megachilidae). Environ. Entomol. *18*, 133–138. https://doi.org/10.1093/ee/18.1.133.
47. Cane, J.H. (2017). Specialist bees collect Asteraceae pollen by distinctive abdominal drumming (Osmia) or tapping (Melissodes, Svastra). Arthropod-Plant Inte *11*, 257–261. https://doi.org/10.1007/s11829-016-9482-4.
48. https://www.discoverlife.org/mp/20q?search=Osmia+lignaria.
49. Vincent, J.F.V. (2001). Cuticle (Encyclopedia of Materials: Science and Technology).
50. Stavenga, D.G., Leertouwer, H.L., Hariyama, T., De Raedt, H.A., and Wilts, B.D. (2012). Sexual Dichromatism of the Damselfly Calopteryx japonica Caused by a Melanin-Chitin Multilayer in the Male Wing Veins. PLoS One *7*, e49743. https://doi.org/10.1371/journal.pone.0049743.
51. Badejo, O., Skaldina, O., Gilev, A., and Sorvari, J. (2020). Benefits of insect colours: a review from social insect studies. Oecologia *194*, 27–40. https://doi.org/10.1007/s00442-020-04738-1.
52. Shamim, G., Ranjan, S.K., Pandey, D.M., and Ramani, R. (2014). Biochemistry and biosynthesis of insect pigments. Eur. J. Entomol. *111*, 149–164.
53. Galván, I., Jorge, A., Edelaar, P., and Wakamatsu, K. (2015). Insects synthesize pheomelanin. Pigm. Cell Melanoma R. *28*, 599–602. https://doi.org/10.1111/pcmr.12397.
54. Gosset, G. (2023). Melanins: Functions, Biotechnological Production, and Applications (Springer Nature).
55. Schroeder, T.B.H., Houghtaling, J., Wilts, B.D., and Mayer, M. (2018). It's Not a Bug, It's a Feature: Functional Materials in Insects. Adv. Mater. *30*, 1705322. https://doi.org/10.1002/adma.201705322.
56. Stavenga, D.G., Leertouwer, H.L., Osorio, D.C., and Wilts, B.D. (2015). High refractive index of melanin in shiny occipital feathers of a bird of paradise. Light Sci. Appl. *4*, e243. https://doi.org/10.1038/lsa.2015.16.
57. Seago, A.E., Brady, P., Vigneron, J.-P., and Schultz, T.D. (2009). Gold bugs and beyond: a review of iridescence and structural colour mechanisms in beetles (Coleoptera). J. R. Soc. Interface *6* (suppl_2), S165–S184. https://doi.org/10.1098/rsif.2008.0354.focus.
58. Deparis, O., Rassart, M., Vandenbem, C., Welch, V., Vigneron, J.P., and Lucas, S. (2008). Structurally tuned iridescent surfaces inspired by nature. New J. Phys. *10*, 013032. https://doi.org/10.1088/1367-2630/10/1/013032.
59. Gebru, A., Rohwer, E., Neethling, P., and Brydegaard, M. (2014). Investigation of atmospheric insect wing-beat frequencies and iridescence features using a multispectral kHz remote detection system. J. Appl. Remote Sens. *8*, 083503. https://doi.org/10.1117/1.Jrs.8.083503.
60. Noh, M.Y., Muthukrishnan, S., Kramer, K.J., and Arakane, Y. (2016). Cuticle formation and pigmentation in beetles. Curr. Opin. Insect Sci. *17*, 1–9. https://doi.org/10.1016/j.cois.2016.05.004.
61. Li, M., Seinsche, C., Jansson, S., Hernandez, J., Rota, J., Warrant, E., and Brydegaard, M. (2022). Potential for identification of wild night-flying moths by remote infrared microscopy. J. R. Soc. Interface *19*, 20220256. https://doi.org/10.1098/rsif.2022.0256.

STAR★METHODS

KEY RESOURCES TABLE

REAGENT or RESOURCE	SOURCE	IDENTIFIER
Deposited data		
Raw data	Current paper	Mendeley Data, V1, https://doi.org/10.17632/tt328cbvmw.1
Experimental models: Organisms/strains		
Osmia californica	NativeBees.com	N/A
Osmia lignaria	NativeBees.com	N/A
Osmia ribifloris	NativeBees.com	N/A
Software and algorithms		
MATLAB	https://matlab.mathworks.com	MATLAB_R2022b
LabVIEW	https://www.ni.com/en-us.html	Version July 2021
Asymmetric Least Squares (AsLS)	This paper[43]	(DOI not found)
Welch's method	This paper[29]	https://doi.org/10.1109/TAU.1967.1161901.
Classification learner	https://www.mathworks.com/help/stats/classification-learner-app.html	Installed App in MATLAB

RESOURCE AVAILABILITY

Lead contact

Requests for further information and resources can be directed to and will be fulfilled by the lead contact of this manuscript, Yiyun Li (yiyunli@tamu.edu).

Materials availability

This study did not generate any new unique materials or reagents.

Data and code availability

- The original datasets for this manuscript have been deposited at Mendeley Data (Mendeley Data, V1, https://doi.org/10.17632/tt328cbvmw.1).
- This paper does not report original code.
- Any additional information required to reanalyze the data reported in this paper is available from the lead contact upon request.

EXPERIMENTAL MODEL AND SUBJECT DETAILS

Solitary native bees used in this study are in the genus *Osmia*, of the family Megachilidae. *Osmia* bees strictly have one generation in a year and are among the earliest emerging bees in spring. Males emerge earlier than females. Some days after mating, females start to forage for pollen and nectar.[44] Images of three species of *Osmia* bees of both genders measured in the laboratory are shown in Figure 1. The total number of individuals we hatched and the number of cocoons we prepared are listed in the bottom right corner. Cocoons of *O. ribifloris* were first kept at room temperature, ~ 73 °F (~ 22.8°C), in the lab with humidity between 62% and 67% (buffered with saturated NaCl solution) for emergence for three days and then switched to ambient lab conditions. Cocoons of *O. lignaria* and *O. californica* were kept for emergence in lab conditions. No special effort was made to regulate the humidity in the lab in this study since *Osmia* spp. are known to be good foragers in damp, cool spring weather as well as dry spring weather. More details about the three species can be found below.

O. ribifloris, also known as the blueberry bee, is native to western North America. They normally gather pollen from plants in the family Ericaceae, with *Arctostaphylos* (manzanita) being a preferred host in the wild. Berberidaceae serve as important alternative pollen hosts if ericaceaeous species are unavailable.[37] *O. ribifloris* has been developed successfully as an efficient pollinator of blueberries in the southern USA.[44] They hatch in the early spring and adult *O. ribifloris* begin foraging at air temperatures as cool as 9°C. The foraging peaks at air temperatures near 21°C – 26°C[38]

O. lignaria, also known as the blue orchard bee, is native to the Pacific Northwest and has become established throughout much of the US due to shipment for pollination.[39] They appear first in early– to mid–May and show a 30 to 35–day activity period.[45] As their nickname

suggests, female individuals of *O. lignaria* are excellent pollinators of apple, pear, and cherry trees and efficient pollinators of fruiting bushes such as blueberries and almonds.[39] They have also been reported collecting pollen from *Arctostaphylos* and the family Asteraceae.[46,47]

O. californica is considered oligolectic with a strong preference for Asteraceae pollens.[46] They hatch a bit later than *O. lignaria* and fly into July.[45]

As shown in Figure 1, *O. ribifloris* individuals are generally metallic–bluish–to–greenish; *O. lignaria* individuals are dark blue and become greenish on the vertex, dorsum of the thorax, and abdominal terga for females and greenish tints on the face, vertex, and dorsum of thorax for males;[48] and *O. californica* individuals are generally black. Males have furry mustaches while females have a dense and elongated scopa on the ventral side of the abdomen for pollen carrying. Per the scale bars, the female individuals tend to be larger than the males.

The survival rate of females was higher than that of males in this study. This indicated that females were less vulnerable to environmental threats, which can be partially explained by the optical information we will discuss later. The extremely low survival rate of *O. ribifloris* males is likely the consequence of initial improper hatching conditions.

METHOD DETAILS

Light–insect interaction

The cuticle is the outer covering of arthropods and is important in shaping the insects' optical properties. It is primarily made of chitin fibers imbedded in a protein matrix.[49] Coloration in insects originates from pigments, cuticular surface structures, or their combination.[50,51]

Melanin is the most common biological pigment and is the only kind of pigment that can be found in the cuticle.[52,53] Melanin reinforces the cuticle through a filler effect.[49] Eumelanin (black to brown) is the main kind of melanin found in insects. Recently, with the help of Raman spectroscopy, pheomelanin (chestnut or yellowish colors) has also been found in insects and later chemically identified.[53] Though, unlike in vertebrates, no melanosomes can be found in insects (invertebrates), it has been reported that melanin granules can be found in insects.[54,55] Melanin pigments contribute to both an insect's coloration and immunological defense. For instance, melanic morphs of *Galleria mellonella* are more resistant to fungal infection than non-melanic ones.[51]

Eumelanin absorbs broadband visible light, and its absorbance decreases rapidly as the wavelength gets longer.[50] Eumelanin absorption does not affect the bands beyond 1200 nm.[24] The refractive index of eumelanin is high (1.7–1.8 in the visible wavelength range).[56] In a quantitative scattering measurement of a well-solubilized eumelanin solution, people found that the scattering from eumelanin with an effective radius of ~38 nm was less than the minimum sensitivity of their instrument at relatively longer wavelengths (325–800 nm).[32] This study suggests that scattering from eumelanin can be neglected when no large melanin granules are formed in the insects. However, the high refractive index of eumelanin still expands its role beyond pure strong absorber. Multilayer structure created by a layered deposition of melanin in a chitin matrix is the cause of the blue wing vein coloration of *Calopteryx japonica* male individuals.[50] The metallic color of *O. ribifloris* and *O. lignaria* should be an outcome of the multilayer reflectors in the insect cuticle. The color reflected depends on the refractive index of the component layers and their periodicity.[57] In a lidar–like remote sensing system, the observation angle is close to normal incidence, and the reflected light from the cuticle would shift towards longer wavelengths.[41,58] Thin–film iridescence of flying insects has been discussed, and the iridescence from the morphological structure on the wings is thought to be the cause of the difference between static reflectance and in–flight spectra of lepidopteran insects.[22,59]

Besides the multilayer reflectors, two other mechanisms also lead to structural color: three–dimensional photonic crystals and diffraction gratings.[60] Structural coloration was also reported from other species. The recently–reported specular reflection from moth wings could be interpreted as a form of diffraction grating consisting of ridges and cross–ribs on the wing.[61] The well–known, circularly polarized light produced by the chiral symmetry of chitin arrays in the cuticle of insects occurs predominately in Rutelinae, Scarabaeinae, and Cetoniinae.[57] Chitin arrays lacking high chirality have a lower impact on the polarization rotation (circular birefringence) process.

The form of eumelanin distribution in the *Osmia* bees and its role in the laser–insect interaction will be partially revealed in the experimental results discussed later. More detailed discussion, e.g., the equivalent absorption pathlength of melanin in the insect body will be reported when we have a better understanding of the laser–insect interaction, e.g., when the structure of *Osmia* bees' cuticle is measured with the scanning electron microscope (SEM), as has been done in.[61]

Experimental setup

The experimental arrangement for optical, multiband, polarimetric modulation, stand-off sensing was inspired by the work of Gebru et al.[24] The scheme of the experimental setup is shown in Figure 2. A flight chamber of size 200×300×400 mm^3 (W×H×L) was built with plexiglass. Two openings of about 55×55 mm^2 were made on both the front and back side to let the laser beams pass through the flight chamber. Multimode lasers at three wavelengths—915 nm (0.42 W, Sheaumann Laser), 1064 nm (0.38 W, Sheaumann Laser), and 1320 nm (0.47 W, SemiNex)—were employed, modulated at a 3 kHz carrier frequency and a duty cycle of 25%. The lasers were vertically polarized and superimposed by a set of two dichroic beam splitters from Semrock. Lasers were collimated by a 25 mm diameter, f300 mm NIR II (750 to 1550 nm) coated achromatic lens from Edmund Optics. The collimating lens was about 2.8 m away from the flight chamber and the laser beams were terminated on black aluminum foil from Thorlabs another ~3.4 m away from the flight chamber.

Backscattered light from flying insects was collected by a 50 mm diameter, f200 mm C–coated achromatic lens from Thorlabs and collimated by a 25 mm diameter, f100 mm lens to pass through the polarizing beam splitter (PBS253, Thorlabs), where the co– and de–polarized backscattered light was separated, and then focused on the detection unit of InGaAs detectors (PDA20CS2, Thorlabs) by 25 mm diameter, f30 mm C–coated achromatic lenses from Thorlabs separately. The photosensitive area of InGaAs detectors is 2 mm diameter, and its

responsivity covers 800 nm to 1700 nm. Since the InGaAs detectors are not sensitive to visible light, no long–pass filters are required in this LED-illuminating indoor measurement. The detectors were imaged on the far side of the flight chamber and the detectors' field of view (FOV) was around 40×40 mm^2. The laser beam profiles of the three lasers were scanned in the horizontal and vertical directions, and the full width at half maximum (FWHM) of the beam profile was used to define the boundary of the FOV at each wavelength. The FOV of the system was defined by the intersection of the FOVs at the three wavelengths, which turned out to be 23 mm horizontally and 27 mm vertically on average. Since the beam of the laser at 915 nm was of the smallest size, the system FOV was mostly determined by the 915 nm beam. The detectors worked at a 60 dB gain setting with a bandwidth of 9 kHz to achieve a balance between a high signal–to–noise ratio (SNR) and a minimized signal residual from the previous time slot. The data from the two InGaAs detectors were collected by a DAQ device (USB 6346, National Instruments) simultaneously. A 12 kHz system clock was generated by a 30 MHz synthesized function generator (DS345, Stanford Research System) and split into four channels with a Johnson decade counter (74HC4017), in the time series of 1320 nm, 915 nm, 1064 nm, and the time slot for background measurement, similar approach has been used in the previous work.[28] The data from the USB 6346 were transferred and saved to a computer by a program written in LabVIEW.

A white LED lamp was mounted on top of the flight chamber to simulate daylight for the bees. A camera (acA1920–155um, Basler) and a 26.1 ° angled mirror, as shown in Figure 2, were introduced for 3D stereo vision, which can help us describe the bees' flight trajectory. Lateral scattered LED light from the insects was collected by an f35 mm lens from Edmund Optics and imaged onto the camera. When an insect was in the FOV, the camera was triggered by the LabVIEW program to operate at a frame rate of 100 fps. In each frame, the center–of–mass pixel numbers were calculated for the insect and its image in the mirror. The center–of–mass pixel coordinates were then converted into 3D coordinates, which were used to represent the insect's position in the FOV. Fresh dandelion flowers were used to stimulate the flight of *O. californica*.

QUANTIFICATION AND STATISTICAL ANALYSIS

The signal intensity was calibrated by randomly dropping a quarter inch (6.35 mm) diameter Teflon ball into the FOV and calculating the average intensity of the recorded Teflon ball signals.

In the average classification accuracy estimate, the training data set (75% of the whole data) and the test data set (25% of the whole data) were chosen randomly. The model training and testing process based on the randomly chosen data sets has been repeated 10 times. The average classification accuracy and its corresponding standard deviation were reported based on the result of these 10 rounds of training–testing process. The training and testing were conducted with the installed Classification Learner app in MATLAB.